

## Observing enzyme ternary transition state analogue complexes by $^{19}\text{F}$ NMR spectroscopy

Anna Ampaw,<sup>a</sup> Madison Carroll,<sup>a</sup> Jill von Velsen,<sup>b</sup> Debabrata Bhattasali,<sup>c</sup> Alejandro Cohen,<sup>d</sup> Matthew W. Bowler,<sup>b</sup> David L. Jakeman<sup>a,c\*</sup>

<sup>a.</sup> *Department of Chemistry, Dalhousie University, Halifax, NS, Canada B3H 4R2.*

<sup>b.</sup> *European Molecular Biology Laboratory, Grenoble Outstation, 71 avenue des Martyrs, CS 90181 F-38042 Grenoble, France*

<sup>c.</sup> *College of Pharmacy, Dalhousie University, Halifax, NS, Canada B3H 4R2. E-mail: [david.jakeman@dal.ca](mailto:david.jakeman@dal.ca)*

<sup>d.</sup> *Proteomics and Mass Spectrometry Core Facility, Life Sciences Research Institute, Dalhousie University, Halifax, NS, Canada B3H 4R2.*

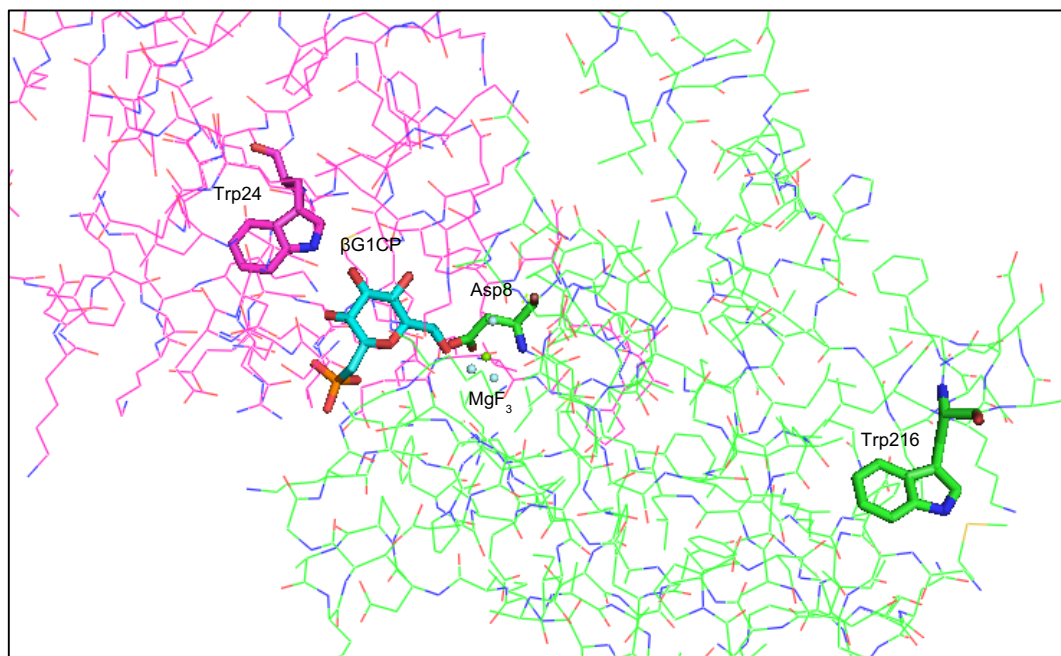


**Fig. S1. Crystal structure of the  $\beta$ PGM-MgF<sub>3</sub>- $\beta$ G1CP TSA complex (4C4R).** The cap domain housing W24 is shown in magenta and the core domain housing W216 is shown in green. Both Trp residues are highlighted with sticks. Asp8 residue responsible for the phosphorylation of the substrate lies on the core domain and  $\beta$ G1CP ligand is positioned in the active site at the interface of both domains. The atoms of MgF<sub>3</sub> are represented with spheres.

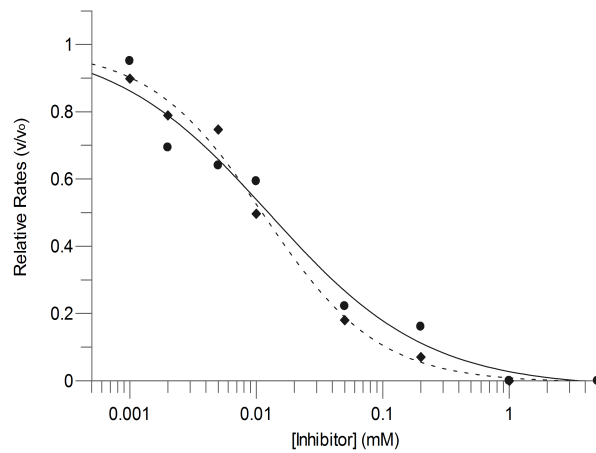


**Fig. S2.** IC<sub>50</sub> plots of  $\beta$ G1CP (circle and solid line) and  $\beta$ G1CF<sub>5</sub>P (diamond and dashed line) as inhibitors of  $\beta$ PGM.

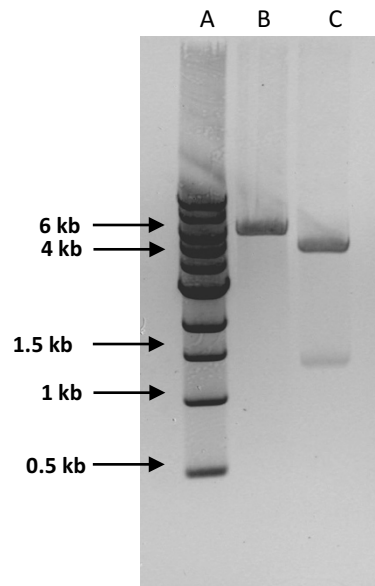


**Fig. S3.** 1% agarose gel of pET-22b *pgmB* and pET-22b *pgmB*-His digested with SacI and PstI. (A) 1 kb DNA ladder; (B) pET-22b *pgmB* digested with PstI and SacI; (C) pET-22b *pgmB*-His digested with PstI and SacI;

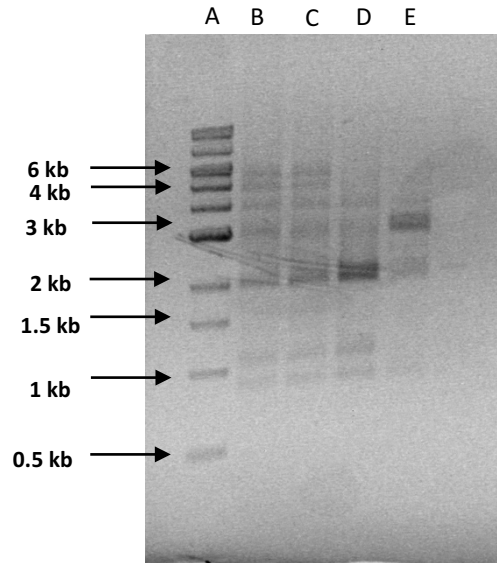


**Fig. S4. 1% agarose gel of pET-22b\_pgmB-His and pET-22b\_pgmB-His\_W24F plasmid digested with BglI and BstEII. (A) 1 kb DNA ladder; (B), (C), (D) pET-22b\_pgmB\_His\_W24F digested with BglI and BstEII; (E) pET-22b\_pgmB digested with BglI and BstEII.**

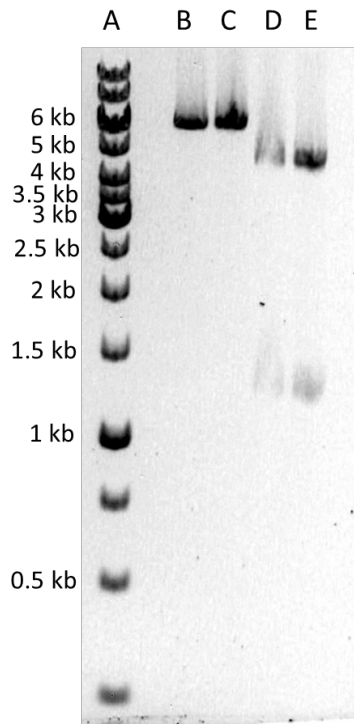


**Fig. S5. 1% agarose gel of pET-22b\_pgmB-His\_W216F plasmid digested with PstI. (A) 1 kb DNA ladder; (B) and (C) pET-22b\_pgmB\_His digested with PstI; (D) and (E) pET-22b\_pgmB\_His\_W24F digested with PstI.**

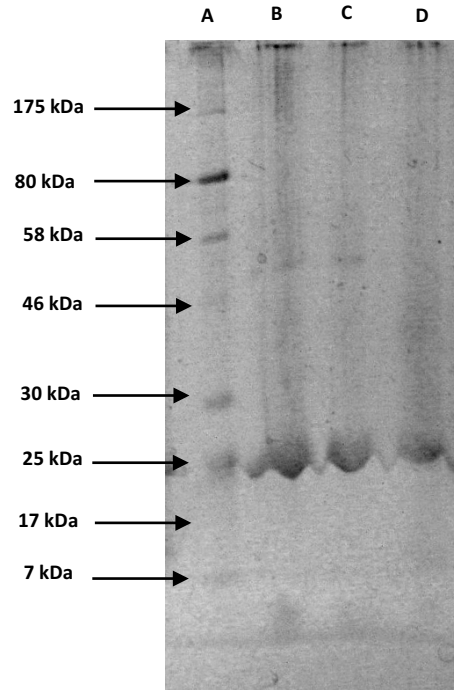


**Fig. S6. SDS-PAGE analysis of  $\beta$ PGM purified from *E. coli* BL21(DE3).** (A) NEB Biolabs broad range prestained protein marker (7-175 kDa); (B) unlabeled  $\beta$ PGM; (C) 5FW $\beta$ PGM expressed with 5-fluorotryptophan (method B) (D) W24F, 5FW $\beta$ PGM expressed with 5-fluorotryptophan (method B).

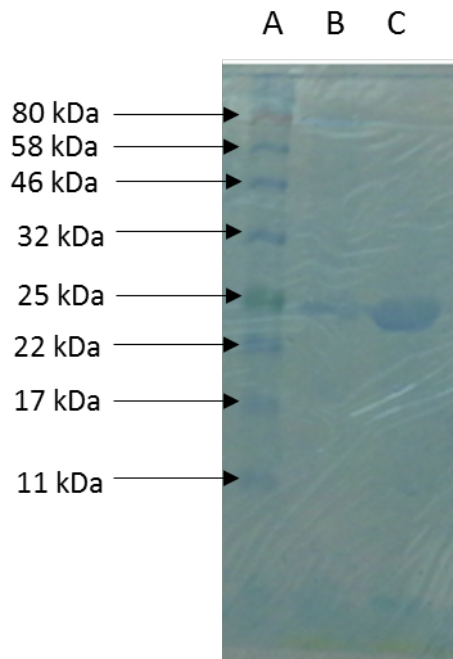


**Fig. S7. SDS-PAGE analysis of 5FW $\beta$ PGM W216F purified from *E. coli* BL21(DE3).** (A) NEB Biolabs broad range prestained protein marker (11-245 kDa); (B) and (C) 5FW $\beta$ PGM W216F (MW= 25 kDa).

## $^1\text{H}$ - $^{15}\text{N}$ HSQC NMR Spectra

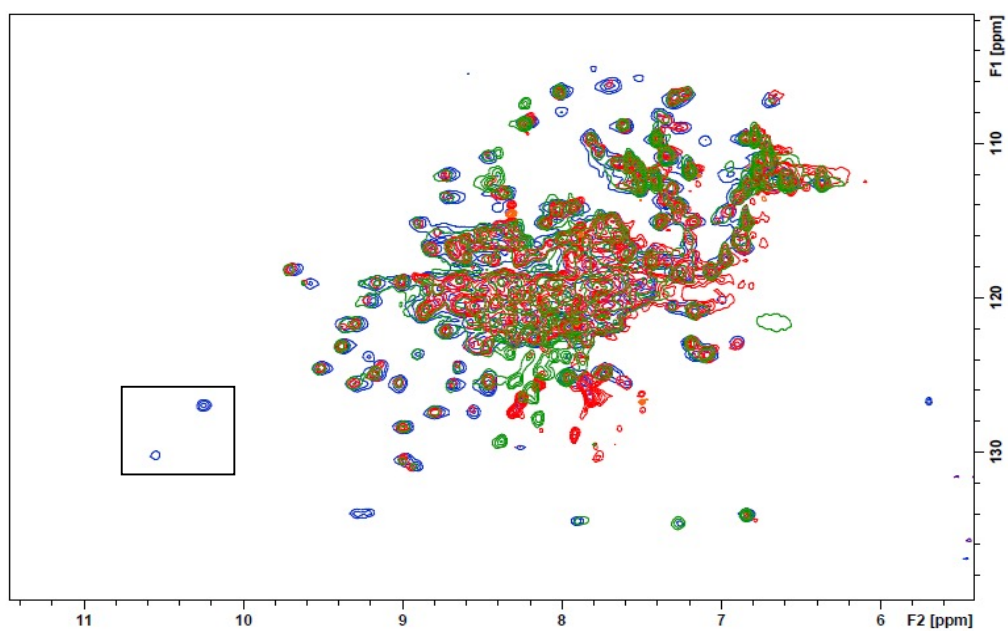


**Fig. S8.** Overlaid  $^1\text{H}$ - $^{15}\text{N}$  HSQC of  $^{15}\text{N}$ -labeled  $\beta\text{PGM}$  (500  $\mu\text{M}$ ) (blue),  $^{15}\text{N}$ -labeled 5FW $\beta\text{PGM}$  from method A (500  $\mu\text{M}$ ) (red) and method B (500  $\mu\text{M}$ ) (green). Both  $^{15}\text{N}$ -labeled 5FW $\beta\text{PGM}$  spectra (red and green) show the absence of cross peak resonances for the side chain Trp residues (black box).

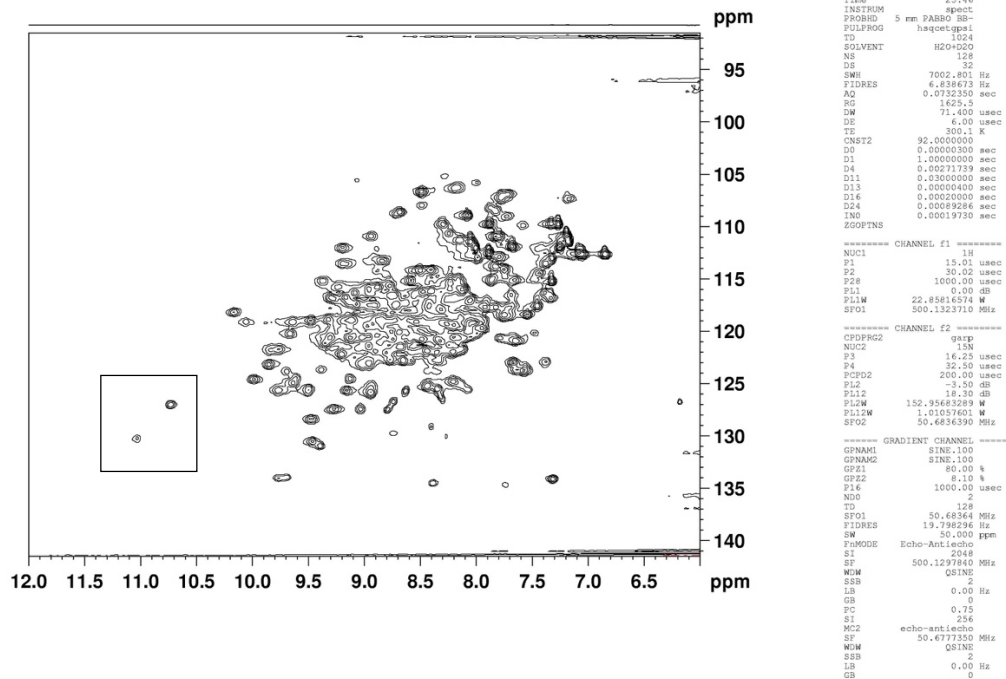


**Fig. S9.  $^1\text{H}$ - $^{15}\text{N}$  HSQC of  $^{15}\text{N}$ -labeled  $\beta\text{PGM}$  (500  $\mu\text{M}$ ).** Cross peaks for W24 and W216 side chain residues are outlined (black box). Enzyme solution contains 5 mM  $\text{MgCl}_2$  and 10%  $\text{D}_2\text{O}$  in 50 mM HEPES pH 7.2.

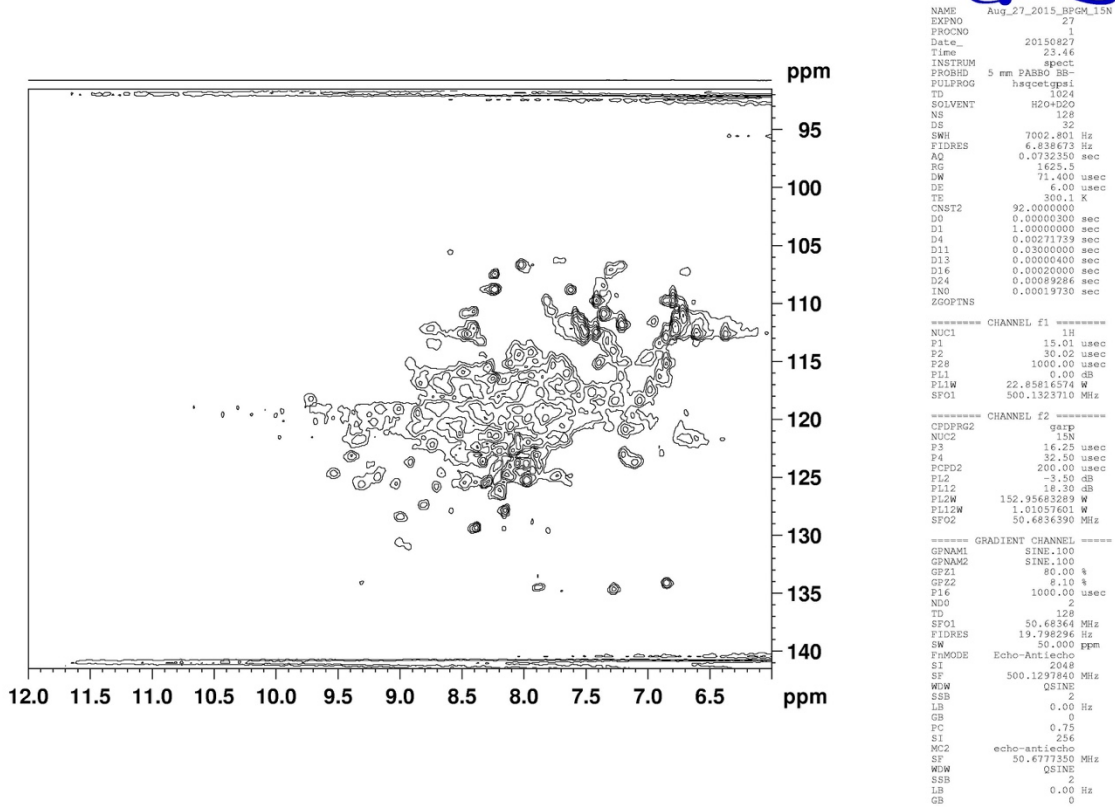


**Fig. S10.**  $^1\text{H}$ - $^{15}\text{N}$  HSQC of  $^{15}\text{N}$ -labeled 5FW $\beta$ PGM from method A (500  $\mu\text{M}$ ). Enzyme solution contains 5 mM  $\text{MgCl}_2$  and 10%  $\text{D}_2\text{O}$  in 50 mM HEPES pH 7.2.

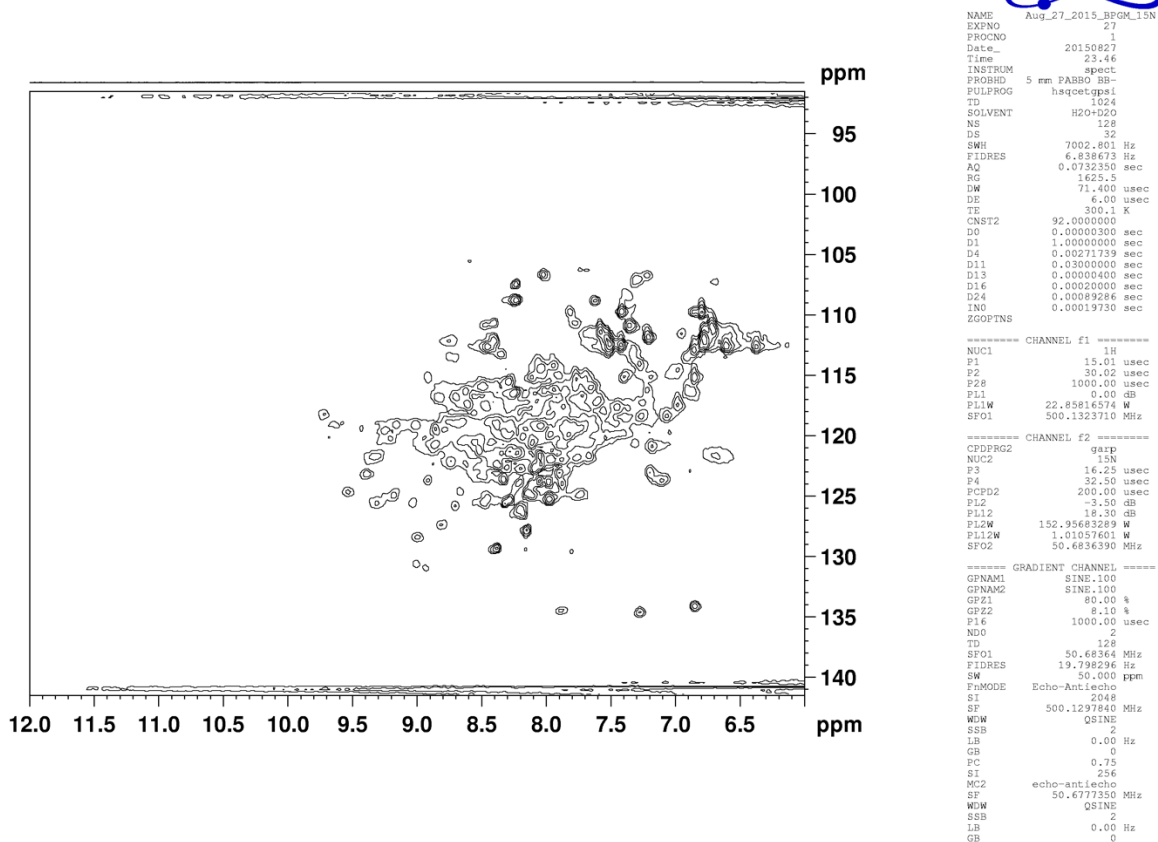


**Fig. S11.**  $^1\text{H}$ - $^{15}\text{N}$  HSQC of  $^{15}\text{N}$ -labeled 5FW $\beta$ PGM from method A (500  $\mu\text{M}$ ). Enzyme solution contains 5 mM  $\text{MgCl}_2$  and 10%  $\text{D}_2\text{O}$  in 50 mM HEPES pH 7.2.



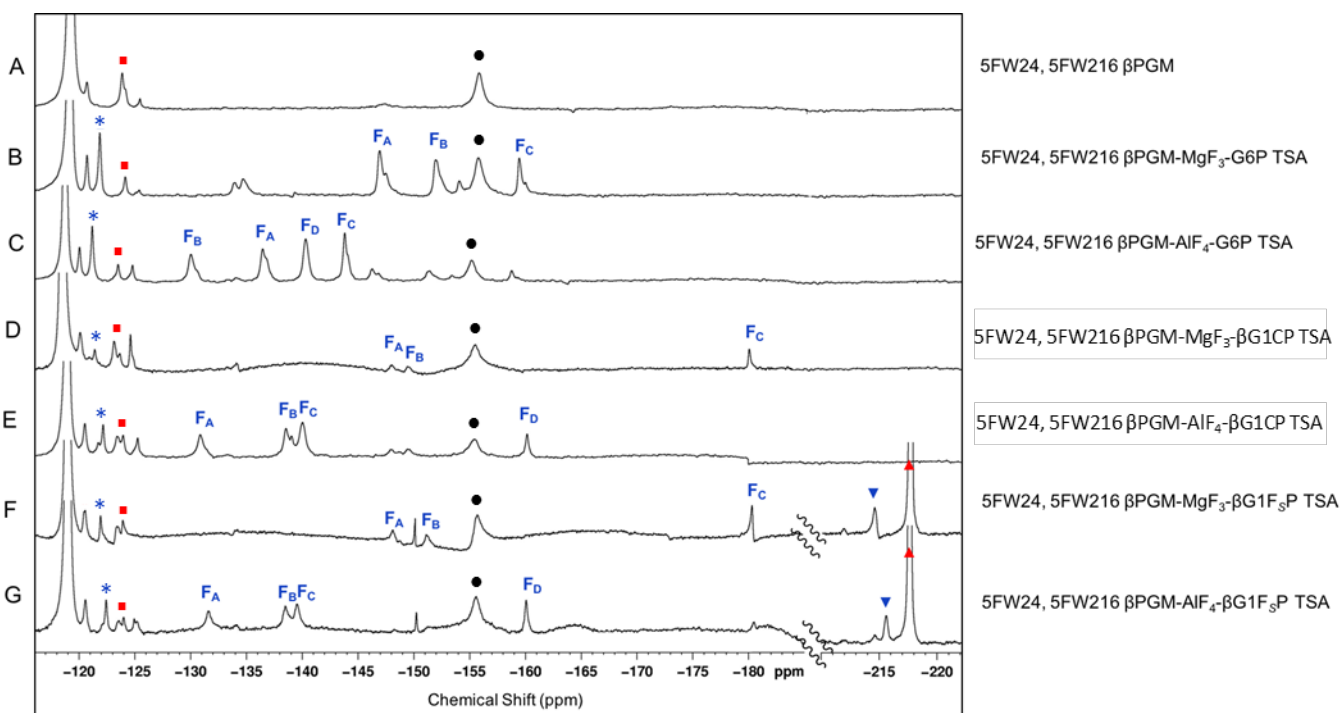


**Fig. S12.**  $^{19}\text{F}$  NMR spectra of step 1 and step 2 TSA complexes with  $^{19}\text{F}$ -labeled wild-type  $\beta\text{PGM}$ . Red boxes (■) are apo-5FW24 resonances, blue asterisks are TSA 5FW24 resonances (\*), black circles (•) are free  $\text{MgF}_3^-$  (-155 ppm), blue inverse triangles (▼) are TSA ligand resonances, and red triangles (▲) are free ligand resonances. Resonances at -119 are from free  $\text{F}^-$ . Assignment of  $\text{MgF}_3^-$  and  $\text{AlF}_4^-$  resonances were previously determined by chemical shift.<sup>3</sup> (A) 5FW $\beta\text{PGM}$ ; (B) 5FW $\beta\text{PGM}$ - $\text{MgF}_3^-$ -G6P TSA2 complex; (C) 5FW $\beta\text{PGM}$ - $\text{AlF}_4^-$ -G6P TSA2 complex; (D) 5FW $\beta\text{PGM}$ - $\text{MgF}_3^-$ - $\beta\text{G1CP}$  TSA1 complex; (E) 5FW $\beta\text{PGM}$ - $\text{AlF}_4^-$ - $\beta\text{G1CP}$  TSA1 complex; (F) 5FW $\beta\text{PGM}$ - $\text{MgF}_3^-$ - $\beta\text{G1CF}_3\text{P}$  TSA1 complex; (G) 5FW $\beta\text{PGM}$ - $\text{AlF}_4^-$ - $\beta\text{G1CF}_3\text{P}$  TSA1 complex; Sample A contains 0.5 mM enzyme, 5 mM  $\text{MgCl}_2$ , 10 mM  $\text{NH}_4\text{F}$ , and 10%  $\text{D}_2\text{O}$  in 50 mM HEPES pH 7.2. Samples B-G contain 1 mM enzyme, 5 mM substrate, 5 mM  $\text{MgCl}_2$ , 10 mM  $\text{NH}_4\text{F}$ , and 10%  $\text{D}_2\text{O}$  in 50 mM HEPES pH 7.2. Samples C, E, and G also contain 1 mM of  $\text{AlCl}_3$ .

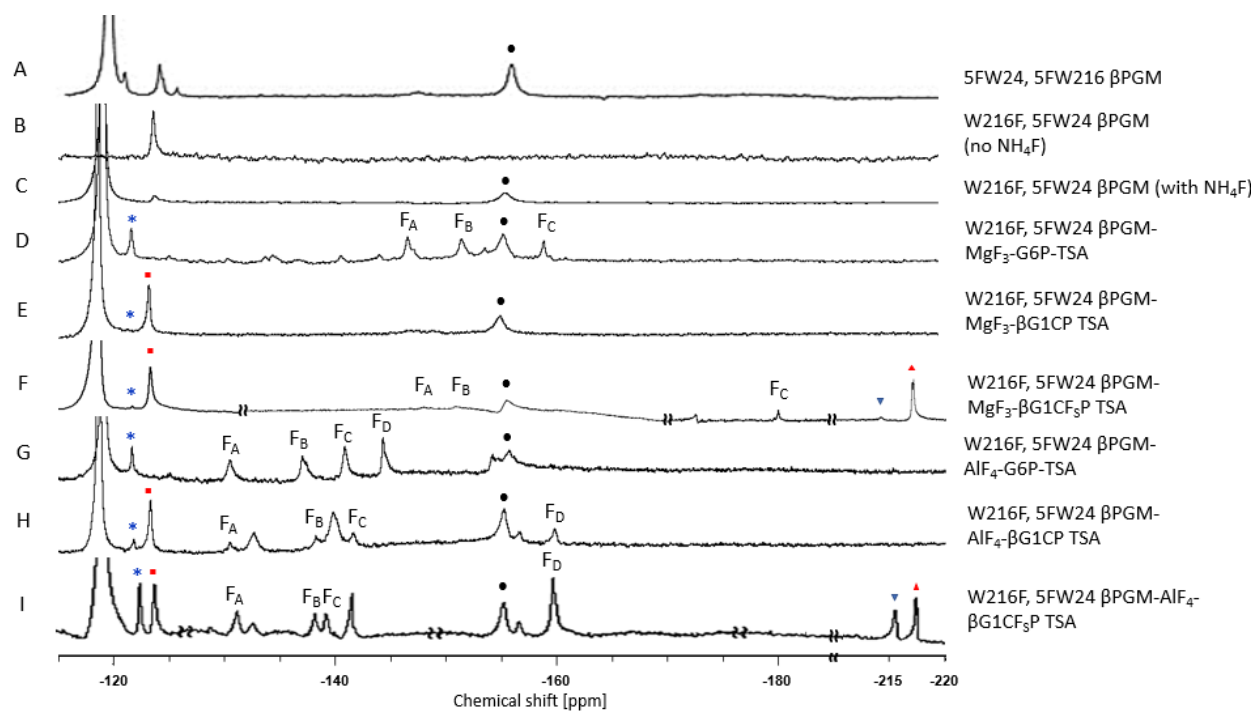


**Fig. S13.**  $^{19}\text{F}$  NMR spectra of the wild-type 5FW $\beta$ PGM, the 5FW $\beta$ PGM W216F mutant, and its TSA1 and TSA2 complexes. Blue asterisks (\*) are TSA 5FW24 resonances, red squares (◻) are apo 5FW24 resonances, black circles (●) are free  $\text{MgF}_3^-$ , blue inverse triangles (▼) are complexed  $\text{G1C}_5\text{FP}$  ligands, red triangles (▲) are free  $\text{G1C}_5\text{FP}$ . (A) wild-type 5FW24 5FW216  $\beta$ PGM; (B) W216F 5FW $\beta$ PGM; (C) W216F 5FW $\beta$ PGM with  $\text{NH}_4\text{F}$  and  $\text{MgCl}_2$ ; (D) W216F 5FW $\beta$ PGM- $\text{MgF}_3$ -G6P TSA2 complex; (E) W216F 5FW $\beta$ PGM- $\text{MgF}_3$ -G1CP TSA1 complex; (F) W216F 5FW $\beta$ PGM- $\text{MgF}_3$ -G1C $_5$ FP TSA1 complex; (G) W216F 5FW $\beta$ PGM- $\text{AlF}_4$ -G6P TSA2 complex; (H) W216F 5FW $\beta$ PGM- $\text{AlF}_4$ -G1CP TSA1 complex; (I) W216F 5FW $\beta$ PGM- $\text{AlF}_4$ -G1C $_5$ FP TSA2 complex.

## LC-MS/MS Data

Liquid chromatography-tandem mass spectrometry (LC-MS/MS) analysis of  $^{19}\text{F}$ -labeled  $\beta\text{PGM}$  was performed for method A (5-fluoroindole incorporation) and method B (5-fluorotryptophan incorporation)  $\beta\text{PGM}$ . Gel bands from SDS-PAGE containing  $^{19}\text{F}$ - $\beta\text{PGM}$  were excised from the gel and rinsed with deionized water. Excised gel bands were processed using Investigator ProGest automated system (Genomic Solutions). Samples were reduced using 100  $\mu\text{L}$  of 10 mM dithiothreitol (DTT), alkylated with 100  $\mu\text{L}$  of 55 mM iodoacetamide and finally digested with Lys-C. The peptides were extracted from the gel pieces by three 20 min incubations with a solution (30  $\mu\text{L}$ ) containing acetonitrile (50%) and formic acid (5%) in LC-MS-grade water with gentle agitation. The extracts were pooled and dried using a vacuum concentrator (Speed Vac Concentrator, SPD 111 V-230, Thermo Electron Corp.) and finally resuspended in LC-MS-grade water (15  $\mu\text{L}$ ) containing acetonitrile (3%) and formic acid (0.5%). LC-MS/MS was performed using a nano flow liquid chromatography system (Ultimate3000RSLCnano, ThermoScientific) interfaced to a hybrid ion trap-orbitrap high resolution tandem mass spectrometer (VelosPro, ThermoScientific) operated in data-dependent acquisition (DDA) mode. 1  $\mu\text{L}$  of each sample was injected onto a capillary column (50cm  $\times$  75  $\mu\text{m}$  PicoTip/PicoFrit Self packed column with Jupiter C18 4u chromatographic media, Phenomenex) at a flow rate of 300  $\text{nL min}^{-1}$ . Samples were electro-sprayed at 1.2 kV using a dynamic nanospray probe. Chromatographic separation was carried out using 90 min linear gradients (Mobile Phase A: 0.1% formic acid in MS-grade water, mobile phase B: 0.1% formic acid in MS-grade acetonitrile,) from 3% B to 35% B over 60 min, then increasing to 95% B over 5 min. MS/MS spectra were acquired using both collision induced dissociation (CID) and higher-energy collisional dissociation (HCD) for the top 15 peaks in the survey 30 000 resolution MS scan. The raw files were acquired (Xcalibur, ThermoFisher) and exported to Proteome Discoverer 2.0 (ThermoFisher) software for peptide and protein identification using SequestHT search algorithm. Extracted ion chromatographs (XICs) were obtained using XCalibur software (ThermoFisher) by screening for specific peptide masses using 50 ppm extraction windows. The intensity of the XIC of peptide fragments containing W24 and 5FW24 (AVLFDLDGVITDTAEYHFRAWK) were compared quantitatively, as well as the peptide fragments containing W216 and 5FW216 (EVWLQK).

For method A, 5FW24 and W24 fragments (Fig. S14) suggested a 5-fluoroindole incorporation of approximately 70%, while 5FW216 and W216 fragments (Fig. S15) suggested a 5-fluoroindole incorporation of approximately 50%. However, in the XIC for the W216 peptide, a peak is seen at 35.50 min, the retention time at which the 5FW216 peptide elutes. We hypothesized that this could be a result of the loss of water from the 5FW216 peptide, therefore exhibiting a mass equal to the W216 peptide. Conclusively, this hypothesis would explain the discrepancy between the values observed. For method B, 5FW24 and W24 fragments (Fig. S16) suggested a 5-fluorotryptophan incorporation of approximately 85%.

5FW216 and W216 fragments (Fig. S17) suggested a similar 5-fluorotryptophan incorporation of approximately 80%, however, similar to method A, a minor peak is seen at 35.03 min, the retention time at which the 5FW216 peptide elutes. Again, this justifies the discrepancy in the values.

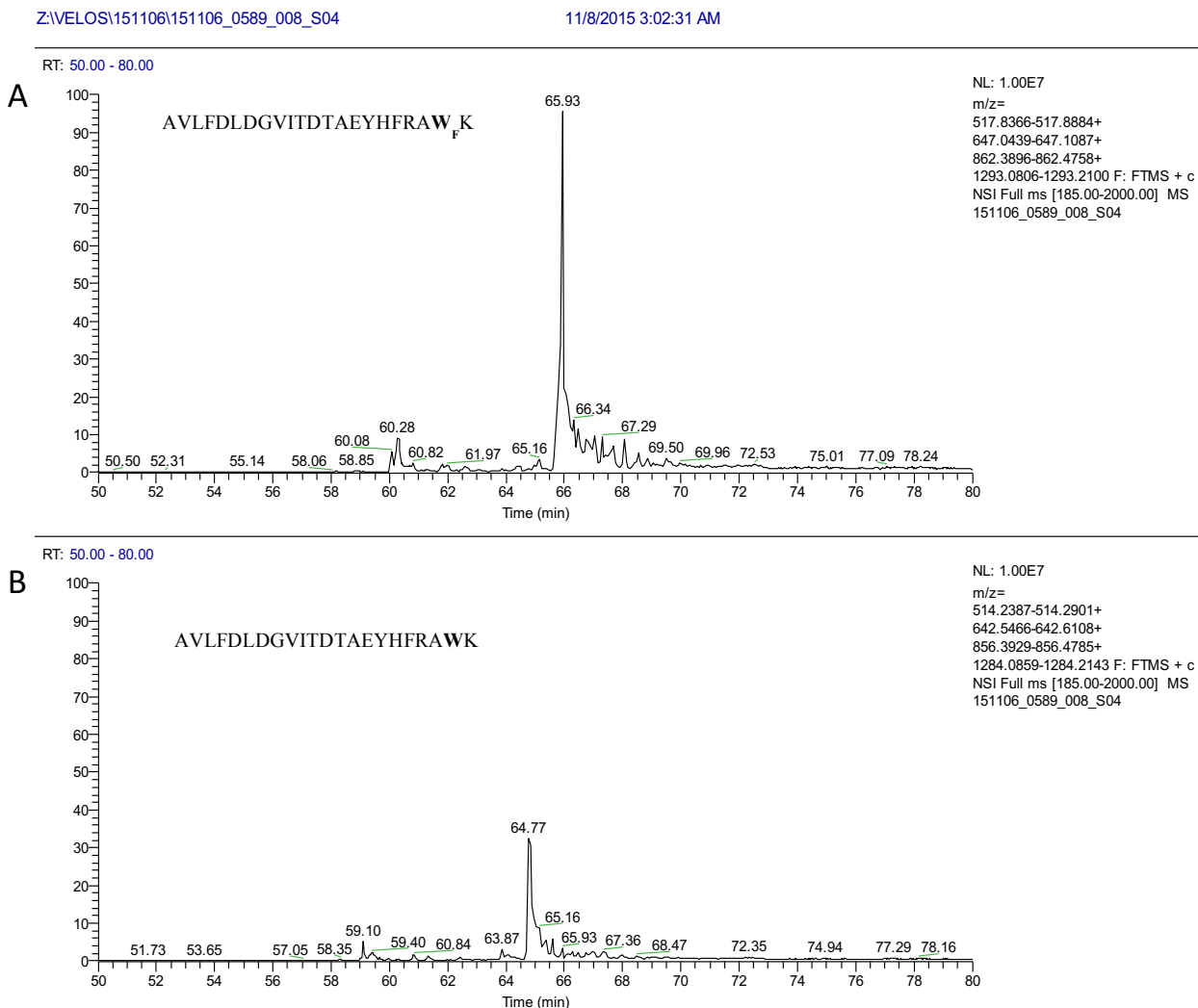


**Fig. S14. Selective XIC of method A <sup>19</sup>F-βPGM showing peptides containing FW24 (A) and W24 (B).** The peak intensity of (B) is approximately 30% the intensity of (A) implying that 70% of the peptide exists in the fluorinated form (FW24). XIC is inclusive of m/z for +2, +3, +4, and +5 charges of peptide and contains a 50 ppm mass window.

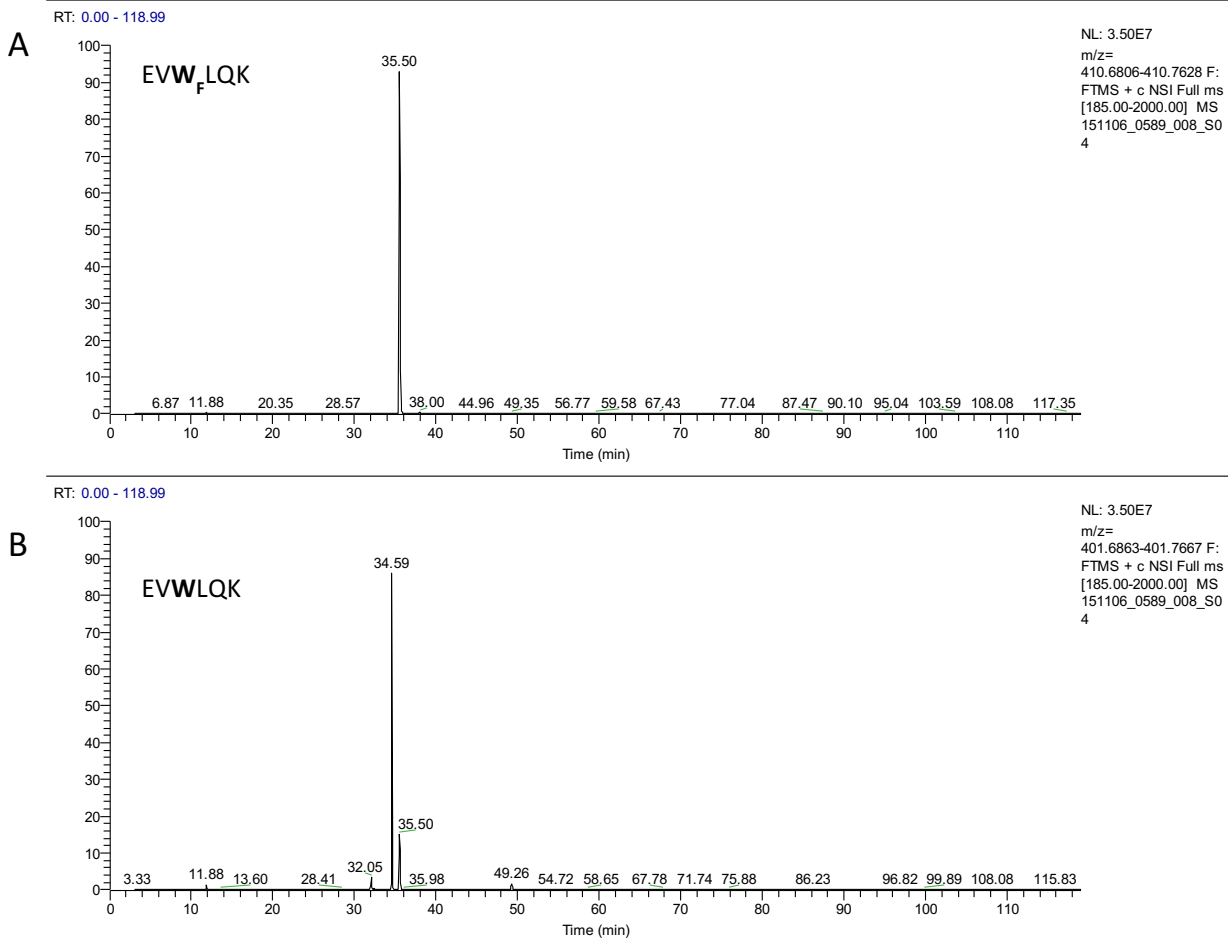
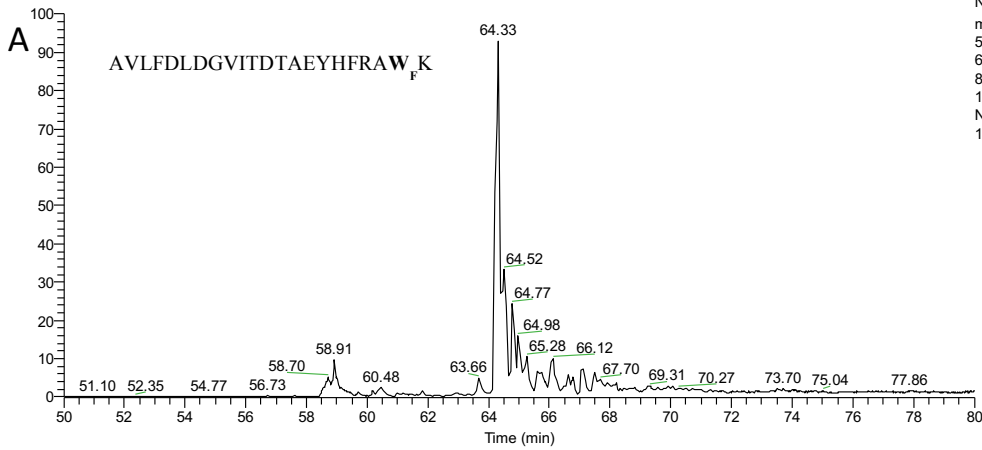


**Fig. S15. Selective XIC of method A  $^{19}\text{F}$ - $\beta$ PGM showing peptides containing FW216 (A) and W216 (B). The peak intensity of (B) is approximately the same intensity as (A) implying that the peptide containing FW24 is present in the same ratio as the peptide containing W24. XIC is inclusive of m/z for +2 charge of peptide and contains a 100 ppm mass window.**

RT: 50.00 - 80.00



RT: 50.00 - 80.00

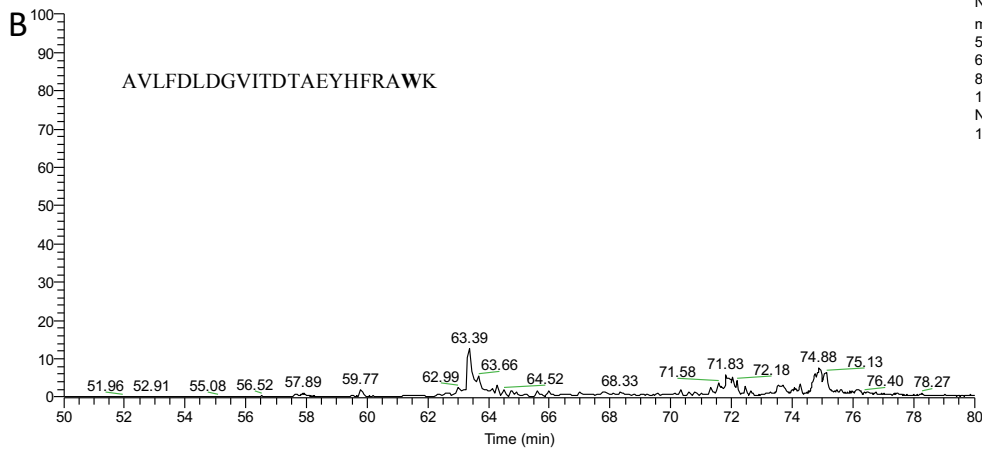


**Fig. S16. Selective XIC of method B  $^{19}\text{F}$ - $\beta$ PGM showing peptides containing FW24 (A) and W24 (B).** The peak intensity of (B) is approximately 15% the intensity of (A) implying that 85% of the peptide exists in the fluorinated form (FW24). XIC is inclusive of m/z for +2, +3, +4, and +5 charges of peptide and contains a 50 ppm mass window.

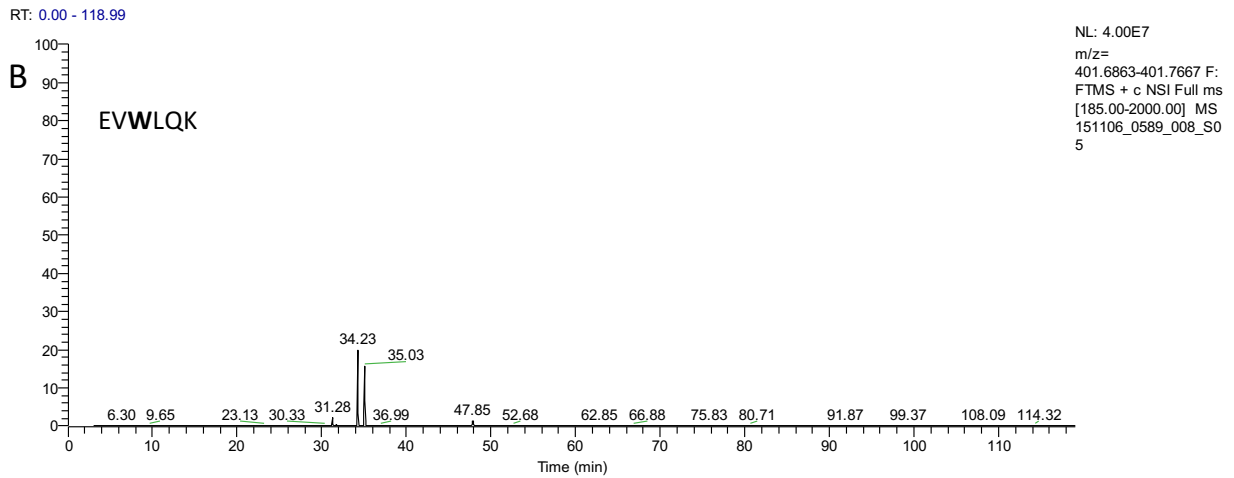
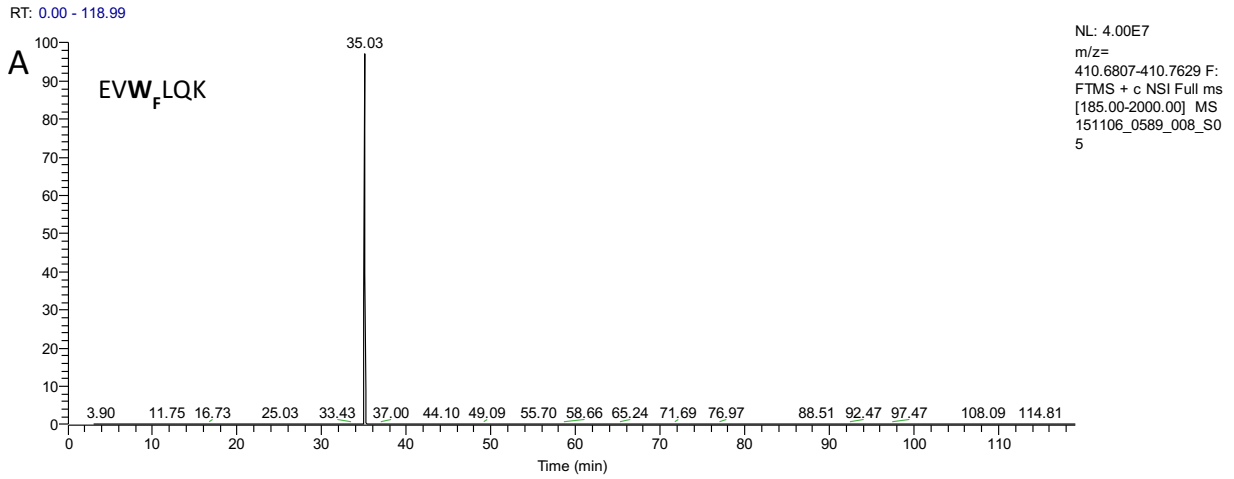


**Fig. S17. Selective XIC of method B <sup>19</sup>F-βPGM showing peptides containing FW216 (A) and W216 (B).** The peak intensity of (B) is approximately 20% the intensity of (A) implying that 80% of the peptide exists in the fluorinated form (FW24). XIC is inclusive of m/z for +2 charge of peptide and contains a 100 ppm mass window.

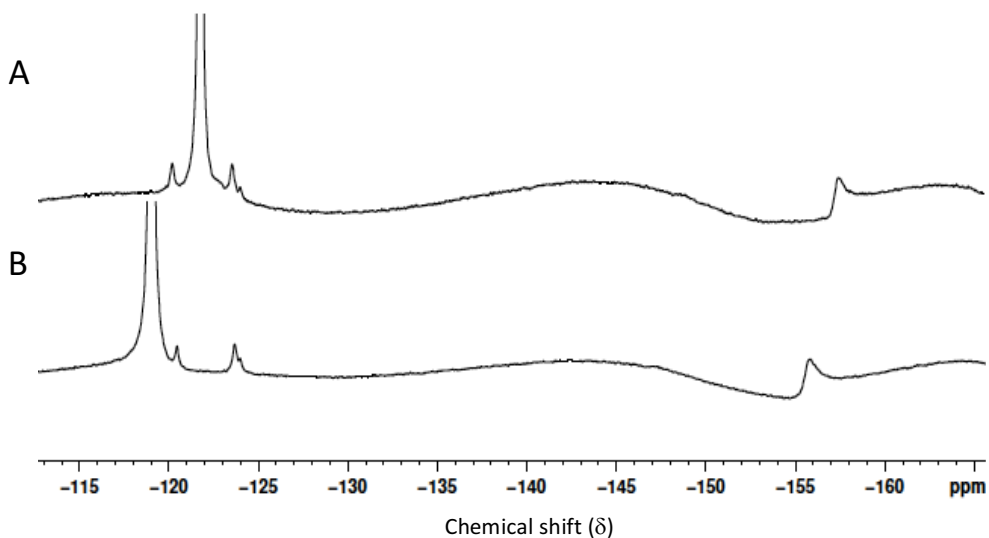


**Fig. S18.**  $^{19}\text{F}$  NMR of 5FW $\beta$ PGM in 100%  $\text{D}_2\text{O}$  (A) and 10%  $\text{D}_2\text{O}$  (B). Samples contain 0.5 mM 5FW $\beta$ PGM, 5 mM  $\text{MgCl}_2$  and 10 mM  $\text{NH}_4\text{F}$ . Sample A contains 50 mM Hepes buffer pH 7.2.

Among the various  $^{19}\text{F}$  NMR spectra that were recorded, we also noticed that the  $\text{F}^-$  ( $\sim$ -119 ppm) and  $\text{MgF}_x$  ( $\sim$ -155 ppm) resonances were not perfectly aligned. We hypothesized that these differences may be a result of solvent induced isotope shifts (SIIS) due to slight variations in the amount of  $\text{D}_2\text{O}$  in each sample. This was confirmed by a  $^{19}\text{F}$  NMR spectra of 5FW $\beta$ PGM in 100%  $\text{D}_2\text{O}$  compared to the  $^{19}\text{F}$  NMR spectra in 10%  $\text{D}_2\text{O}$  (SI, Fig. S16). The  $^{19}\text{F}$  NMR spectra exhibited a 2.8 ppm change in chemical shift upfield for the  $\text{F}^-$  resonance and a 1.7 ppm change in chemical shift upfield for the  $\text{MgF}_x$  resonance, while the chemical shifts for 5FW24 and 5FW216 only exhibited minor changes (0.1-0.2 ppm). The proportions of the two resonances observed for 5FW216 were also not affected by the increase in  $\text{D}_2\text{O}$  in the sample suggesting that a second resonance observed for 5FW216 is not a result of SIIS.



**Table S1** Data collection and refinement statistics

	<i>Apo-protein</i>	<i>5FW8PGM-MgF<sub>3</sub><sup>-</sup>-G6P complex</i>	<i>5FW6PGM-MgF<sub>3</sub><sup>-</sup>-G6P complex</i>
PDB code	5OLW	5OLX	5OLY
X-ray source	MASSIF-1 (ESRF, France)	MASSIF-1 (ESRF, France)	MASSIF-1 (ESRF, France)
Number of images	887	2660	2280
Oscillation step (deg)	0.15	0.05	0.05
Wavelength (Å)	0.966	0.966	0.966
Exposure per frame (s)	0.196	0.02	0.02
<b>Indexing and Scaling</b>			
Space group	<i>P</i> 2 <sub>1</sub> 2 <sub>1</sub> 2	<i>P</i> 2 <sub>1</sub> 2 <sub>1</sub> 2 <sub>1</sub>	<i>P</i> 2 <sub>1</sub>
Unit cell dimensions a, b, c (Å)	a = 61.0, b = 73.9, c = 120.4	a = 37.5, b = 54.2, c = 104.2	a = 57.7, b = 36.7, c = 107.8
α, β, γ (°)	90, 90, 90	90, 90, 90	90, 105.3, 90
Resolution Range (Å)	47.22 -2.28	52.1 – 1.38	44.47 – 2.01
Wilson B-factor (Å <sup>2</sup> )	28.52	9.14	11.52
Completeness (%)	99.7	98.0	91.9
I over Sigma (I)	8.9	6.7	10.9
Multiplicity	3.9	4.8	2.8
<b>Refinement</b>			
Resolution Limits (Å)	20.0-2.28	20.0-1.38	20.0-2.01
R <sub>work</sub> /R <sub>free</sub> (%)	20.25/26.59	15.03/19.29	21.25/25.82
Bond lengths (Å)	0.013	0.008	0.013
Bond Angles (deg)	1.337	1.068	1.292
Average B-factor (Å <sup>2</sup> )	46.98	13.95	17.60
Ramachandran favored (%)	95.0	97.8	97.0
Ramachandran outliers (%)	1.3	0.0	0.0
Clashscore	7.90	2.00	5.21

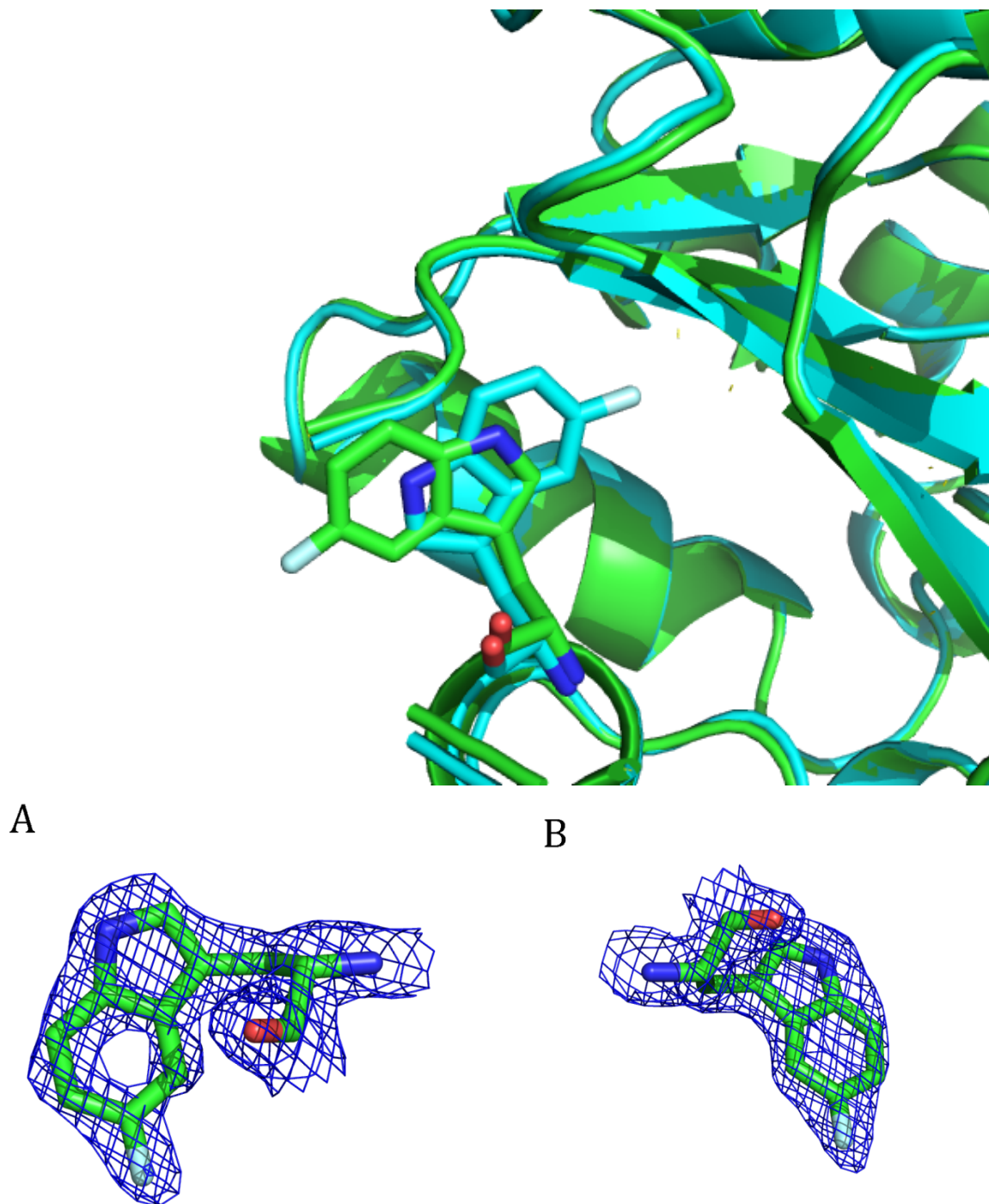


**Figure S19. Alternative conformations of 5FW216 observed in the monoclinic crystal form.** Top: The two molecules on the asymmetric unit are superimposed showing the alternative orientations. The protein adopts exactly the same conformation but can accommodate the two positions of 5FW216. Bottom: Electron density (blue mesh contoured at  $1.5\sigma$ ) for the 2 conformations observed for 5FW216 in the monoclinic crystal form of the closed conformation structure of  $\beta$ PGM. The two molecules in the asymmetric unit show different conformations of the labelled amino acid.

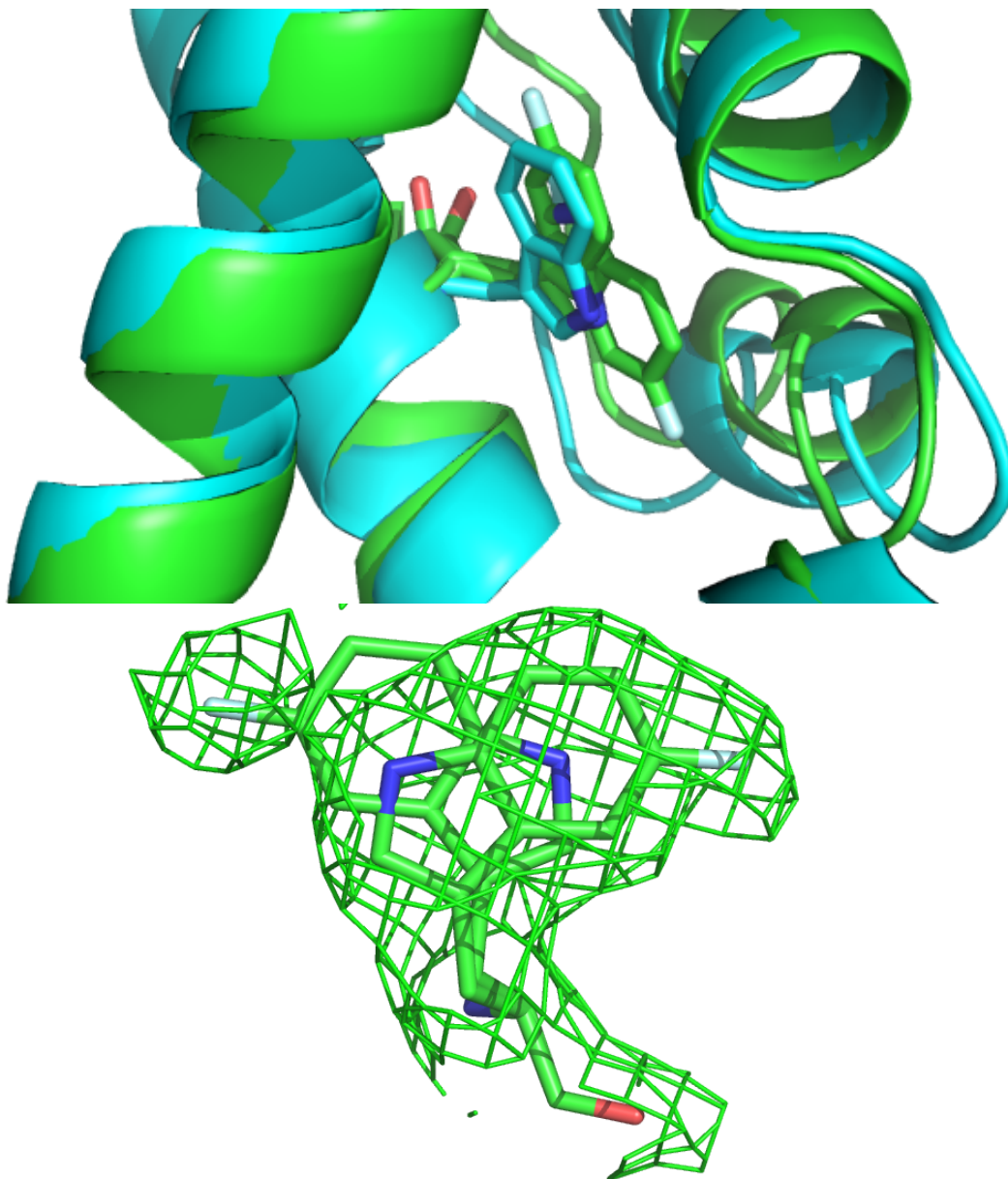


**Figure S20. Alternative conformation of 5FW24 in the cap domain of the open structure.** Top: The open structure of 5FW $\beta$ PGM (green) is shown aligned to the open unlabeled structure (cyan). An alternative conformation is observed for the 5FW24, not seen in the unlabeled protein. The occupancy of the alternative conformation is very low (10%). Bottom: Simulated annealing omit map (green mesh contoured at  $2.5\sigma$ ) showing the density for 5FW24 in the open apo-structure of  $\beta$ PGM. The second conformation is at an occupancy of 10%